Element zonation in carbonated alkali-activated slag

Nedeljkovic, Marija; Zinngrebe, Enno; van der Laan, Sieger; Ghiassi, Bahman; van Hoek, Corrie; Melzer, Stefan; Ye, Guang

Publication date
2018

Document Version
Final published version

Published in
Conference in honor of Centennial of laboratory of construction materials and 60th Birthday prof. Karen Scrivener

CONFERENCE IN HONOR OF

Centennial of

LABORATORY OF CONSTRUCTION MATERIALS

and

60th Birthday Prof. Karen Scrivener

Book of Abstracts

19-20-21-22 August 2018

Lausanne, Switzerland

lmc.epfl.ch

100 ans 1918-2018
ÉCOLE POLYTECHNIQUE FÉDÉRALE DE LAUSANNE

ELEMENTAL ZONATION IN CARBONATED ALKALI-ACTIVATED SLAG

M. Nedeljković[1], E. Zinngrebe[2], S. van der Laan[2], B. Ghiassi[1], C. van Hoek[2], S. Melzer[2], G. Ye[1]

[1] *Microlab, Faculty of Civil Engineering and Geosciences, Delft University of Technology, Stevinweg 1, 2628 CN Delft, The Netherlands.*

[2] *Tata Steel, R&D, P.O. Box 10.000, 1970 CA IJmuiden, The Netherlands.*

Introduction

Durability of alkali-activated materials (AAMs) has received increasing attention from the research and engineering communities over the past decade, because it has critical influence on the prediction of the service life of reinforced concrete elements made of AAMs. Carbonation is one of the major causes for the corrosion of steel rebar embedded in concrete. Compared to ordinary Portland cement (OPC), in alkali-activated slag (AAS), carbonation is not yet fully understood in spite of many studies on the effect of various parameters on carbonation resistance of AAS [1, 2]. The obtained data from the service [3] and laboratory [4] in terms of carbonation resistance of AAS are contradictory. When cured in sealed conditions prior exposure, AAS exhibited high carbonation resistance [5], however, it is unknown whether the same resistance can be expected for unsealed cured pastes. The latter is practically more relevant and many laboratory studies reported poor performance [4, 6]. This study was performed to gain a more fundamental understanding of the carbonation mechanism of AAS. To clarify the carbonation mechanism, chemical characterization of microstructure of naturally carbonated AAS is performed.

Materials and sample preparation

The chemical composition of the ground granulated blast furnace slag (GBFS) used in this paper is 39.8 % CaO, 35.5% SiO_2, 13.5% Al_2O_3, 8.0 % MgO, 1.0% S, 1.0% TiO_2, 0.6% Fe_2O_3, 0.5% K_2O, 0.4% Na_2O. The alkaline activator was prepared by mixing anhydrous pellets of sodium hydroxide with deionized water and commercial sodium silicate solution (27.5 wt.% SiO_2, 8.25 wt.% Na_2O). The activator concentration was 4.8 g Na_2O per 100 g GBFS. The alkaline activator to GBFS ratio was 0.5. The pastes for carbonation study were cast in cylinders with 35 mm diameter and height of 70 mm. The pastes were cured for 28 days in sealed and unsealed conditions (99% RH, ambient temperature) before exposure. After 28 days, the AAS pastes were exposed in natural laboratory conditions, in 0.038 vol. % CO_2 at 20°C and 55% RH for 2 years.

Methods

The microstructure of AAS was characterized with Optical Microscope (Zeiss AxioImager, transmitted light) and Field Emission Scanning Electron Microscope (FE-SEM) (JEOL JSM7001F, with operating conditions of 15 keV and 6 nA). Elemental changes were studied with energy dispersive X-ray spectroscopy (EDS, dual SDD and NSS 3.3). Extraction of the elemental profiles was done by segmentation of the profile brightness intensity of element maps, which is related to the number of the counts collected with EDS detector. The use of concentrations based on averaged brightness intensities of element maps instead of widely used quantitative EDS analysis is accordingly: *i*) EDS analysis are standardless and normalized to 100% (unless analyses are calibrated with standards, which is rare) ; *ii*) density differences caused by porosity, or from CO_2 addition, remains unnoticed by quantitative EDS analysis, except by deviant ZAF correction effects they cause ; *iii*) the absolute amount of element characteristic X-rays per volume area is faithfully represented in element maps, showing effects of material loss and carbonation in lowered intensities. For quasi-local averaging, the EDS map was cut in 250 pixels (~ 250×820 μm^2) blocks and average intensity was measured per block using Axiovision 4.8 software (Zeiss). The unreacted GBFS particles, voids, microcracks were eliminated by image segmentation and only counts from reacting part (gel) were used for EDS profiling. The examined length was 9.5 mm long and 0.82 mm wide. XRD phase identification was performed with a Bruker D4 diffractometer. The Rietveld quantification of the phases was done with TOPAS. WDXRF measurements were done with Panalytical AXIOS Max Advanced XRF spectrometer.

Results

The mosaic of unsealed cured AAS paste after 2 years of exposure is shown in Fig. 1, with red lines indicating the position of the EDS-mapped area ("ribbon"). It was found in authors' previous study, that unsealed curing conditions resulted in substantially reduced Na concentration in the pore solution of the AAS pastes [7]. While no carbonation was found after 2 years in sealed cured paste (first 28 days sealing, and then paste samples were unmoulded and kept 2 years in laboratory conditions), the carbonation does occur in unsealed cured paste. Propagation of the carbonation front was presumably controlled by the ingress of CO_2 into the pore system by diffusion, with a concentration gradient of carbon dioxide as a driving force [8].

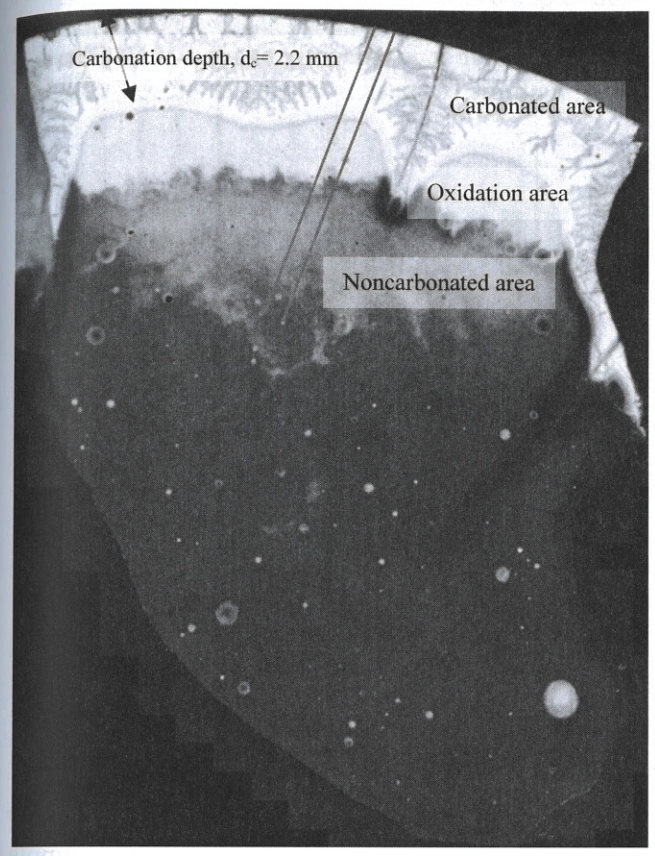

Fig. 1: Mosaic of unsealed cured AAS paste after 2 years of exposure to natural laboratory carbonation determined with Optical Microscope. The red lines indicate location of the extracted maps.

The gel in AAS was carbonated only near the surface to 2.2 mm depths after 2 years, followed by the oxidized and noncarbonated zones. The noncarbonated and carbonated microstructures are shown in Fig. 2. The volume proportion of the angular GBFS particles seems clearly higher in the carbonated area. The difference is attributed to processes which subsequently occurred during the 2 years such as leaching of Na in the curing period (first 28 days), drying after samples were moved from the curing room to laboratory conditions, and natural carbonation. Na-leaching during curing and subsequent ingress of CO_2 changed the near surface area of the sample, such that the dissolution of GBFS grains was restricted compared to the core of the sample. Due to sample polishing and use of high vacuum for SEM imaging, the artificial microcracks are observed in noncarbonated microstructure (Fig. 2), although in Fig. 1 under high magnification (not shown here), they were not present. Carbonation was sporadic as it can be seen in the Fig. 2. Depending on the local gel structure, i.e. Ca/Si ratio and gel porosity carbonation will be enhanced by microcracks such as demonstrated in Fig.1, where carbonation follows the microcrack paths. The oxidation area had less apparent microcracks, however those observed seemed induced by drying.

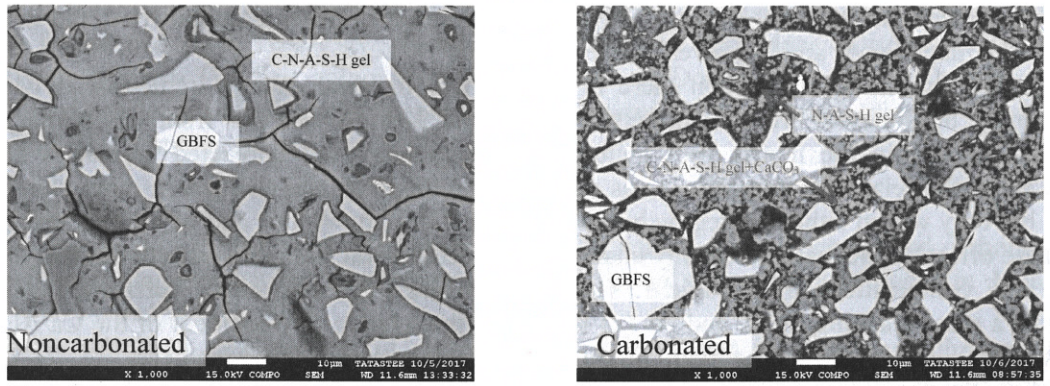

Fig. 2: SEM-BSE images of noncarbonated (sample core) area, b) carbonated (surface) area.

The image brightness profiles shown in Fig. 3 result from a combination of two factors, composition change and material density change, together giving rise to the chemical profiles for C, Na, Al, Si, S, Ca. The locations where changes occur (Fig. 1) are reflecting the behaviour of individual elements in these areas (Fig. 3) as presented by change in colour intensity. In the greyscale image, an abrupt density change corresponds to the transition from the bright to the dark area, the noncarbonated area being denser than the carbonated. Looking at the Ca changes along the profile, the Ca intensity is reduced in the carbonated compared to the noncarbonated area, and changes significantly. Several distinct reaction fronts are noticed, showing independent behaviour of Ca, Na, S, corresponding to: carbonation (I), Ca, Na-dissolution (II), and two sulfurization fronts (III, IV).

Fig. 3 shows that S is accumulating just after the local Na-peak in the Na profile (indicated by the two characteristic S-peaks), being enhanced in entire oxidation area. Presumably, the pore solution in the

oxidation area was saturated by sulphates that precipitated in the microstructure. Possibly, the depletion is from such a large area that it cannot be noticed here, while the enrichment in a specific layer is noticeable because the high levels it reached. But clearly it is difficult to explain why S has the same apparent level before and after the enrichment zone. For Na, it can be seen that is severely leached at the surface, however enriched in the area where Ca is dissolving (front II). S and Na behave independently of the carbonation, and although Na- and S-peaks are close, they are not coinciding, with the Na-peak occurring shallower than S in the profiles.

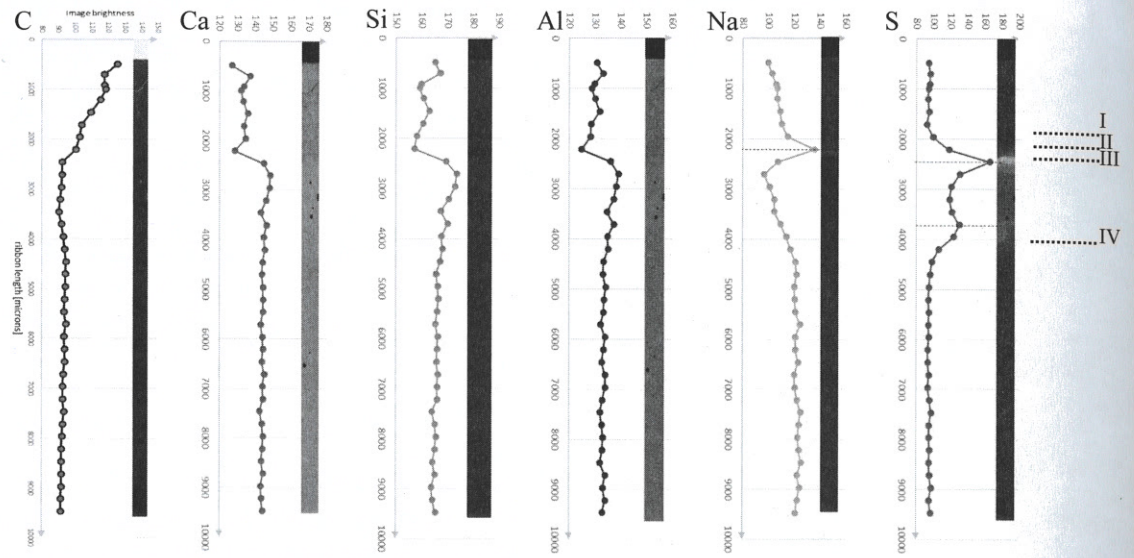

Fig. 3: Averaged brightness profiles of the EDS elemental maps.

Carbon increases at the surface and it drops gradually toward the dissolution front. Since an entire net of microcracks is found at the surface, carbon is mainly resulting from the epoxy which was used for sample preparation. Additionally, carbon is in general difficult to analyse with the SEM-EDS due to its low characteristic X-ray yield. It appears as if oxygen is less present in the surroundings of the microcracks, which is difficult to explain since its profile combines several effects (sulphur oxidation, carbonation, water loss). Mg, Al, Si, Ca had similar behaviour along the profile, and they all were affected by the carbonation. Separately, Si-behaviour was very close to Ca with a drop larger in the dissolution front and in carbonated areas, while the maps for Al and Mg reveal the least changes.

It is assumed that along the ribbon there is one primary material change front, that is where all the elemental image brightnesses drop down, between 2200 and 2400 μm. At this front, the primary change is that material density in the matrix (not including the segmented-out unreacted grains) is significantly lowered. Taking the relatively immobile Al as a reference, compositional changes in other elements can be evaluated, but only within either the region below or above 2300 μm. Above and below this level, the image intensities are offset by the material density change, as reflected in the comparison between image brightness and local XRF compositions from Table 1. Thus, the profiles show two major horizons, level III as the beginning of a mass leaching of Ca and Na (as shown by the relative development of the Ca/Al and Na/Al brightness ratios), and level I as the beginning of the reprecipitation of these elements, i.e. the carbonation horizon, where the material density significantly decreases. The two horizons are coupled as a dissolution – reprecipitation pair, where elements are transported from the inner dissolution zone to the outer reprecipitation zone. The reduced material density in the carbonated part may have involved net material growth, i.e. expansion of the outwardly unconfined sample. Unfortunately, dimensional changes of the sample were not accurately recorded. In principle, a bulk volume expansion of the outer carbonated zone, compared to the core, could be demonstrated by measuring the average interparticle distances between inert GBFS grains assuming they are homogeneously distributed throughout the sample. However, there is a considerable difference in the degree of reaction of GBFS grains in core and rim (Fig. 2). Hence it is difficult to establish how distances between remaining grains should be compared, and this method has not been applied.

Looking in the XRF analysis (Table 1), the difference between noncarbonated (ref) and carbonated areas was mainly in Na_2O, while other elements were similar in both areas. It implies that elements that are dissolved under carbonation were transported to pore solution of the sample, i.e. in the gel pores. The reduced Na_2O content stems from the leaching as found in [7]. Higher Na_2O amount is found in carbonated

area, due to tendency of Na to diffuse toward the surface, as it can be seen from the Fig. 3. Amount of iron increased in reference sample, in agreement with XRD phase identification present in magnetite. Magnetite appears due to contamination of the sample during preparation (Fig. 4). Carbonation products were predominantly aragonite with minor calcite.

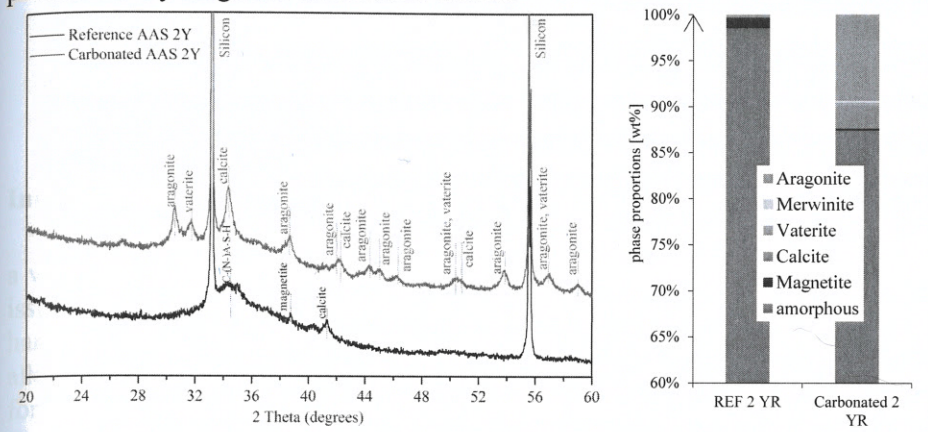

Table 1	Ref	Carb
Na_2O	3.33	4.14
MgO	5.52	5.22
Al_2O_3	8.86	8.70
SiO_2	32.60	32.57
SO_3	1.37	1.40
K_2O	0.32	0.39
CaO	41.51	43.42
TiO_2	1.37	1.49
MnO	0.38	0.45
Fe_2O_3	4.32	1.66

Fig. 4: XRD diffractograms with respect to phases in reference AAS and carbonated bulk AAS pastes after 2 years of exposure to natural carbonation (left). Reference powder diffraction files (PDF#) from ICSD database: Aragonite (PDF# 41-1475), Vaterite (PDF# 33-268), Calcite (PDF# 47-1743), Magnetite (PDF# 65339). Quantitative phase analysis by Rietveld method (middle). WDXRF measurements (right).

Conclusions

Na^+ leaching from the pore solution in the first 28 days and microcracking favoured carbonation reactions in the unsealed cured AAS paste. Elemental mapping profiles indicated that Na, S and Ca show the most distinct spatial distributions. From the sample surface towards the noncarbonated core several fronts were identified: carbonation, dissolution, oxidation and sulfurization fronts. The main crystalline carbonation phases in natural carbonated AAS were aragonite and calcite, with a total of 5.28 wt.% bound CO_2. The importance of proper curing should be underlined for improved carbonation resistance of AAS.

ACKNOWLEDGEMENTS: This research was carried out under the project S81.1.13498 in the framework of the Partnership Program of the Materials innovation institute M2i (www.m2i.nl) and the Technology Foundation STW (www.stw.nl), which is part of the Netherlands Organisation for Scientific Research (www.nwo.nl). The first author thanks Frank van der Does for his help with experiments. The fourth author acknowledges the financial support of the European Union's Marie Curie Individual Fellowship program under REAgrant agreement No. 701531.

REFERENCES:

[1] S.A. Bernal, J.L. Provis, R.M. De Gutiérrez and J.S. van Deventer. Accelerated carbonation testing of alkali-activated slag/metakaolin blended concretes: effect of exposure conditions, in Materials And Structures, vol. 48, p. 653-669, 2014.

[2] S.A. Bernal, R.M. de Gutierrez, J.L. Provis and V. Rose. Effect of silicate modulus and metakaolin incorporation on the carbonation of alkali silicate-activated slags, in Cement And Concrete Research, vol. 40, p. 898-907, 2010.

[3] C. Shi, D. Roy and P. Krivenko. Alkali-activated cements and concretes, in CRC press, 2006.

[4] N. Li, N. Farzadnia and C. Shi, Microstructural changes in alkali-activated slag mortars induced by accelerated carbonation, in Cement And Concrete Research, vol. 100, p. 214-226, 2017.

[5] M. Nedeljković, Y. Zuo, K. Arbi and G. Ye. Carbonation resistance of alkali-activated slag under natural and accelerated conditions, in Journal of Sustainable Metallurgy, vol. 4, p. 33-49, 2018.

[6] M. Palacios and F. Puertas. Effect of Carbonation on Alkali-Activated Slag Paste, in Journal of the American Ceramic Society, vol. 89, p. 3211-3221, 2006.

[7] M. Nedeljković, B. Ghiassi, S. van der Laan and G. Ye. Effect of curing conditions on the pore solution and carbonation resistance of the alkali-activated fly ash and slag pastes, in Cement And Concrete Research, 2018. Submitted.

[8] B. Johannesson and P. Utgenannt. Microstructural changes caused by carbonation of cement mortar, in Cement And Concrete Research, vol. 31, p. 925-931, 2001.